Study of the Boundary Layers in Chemical Laser Nozzles

Richard J. Driscoll*
Bell Aerospace Textron, Buffalo, N.Y.

Chemical laser nozzles, both axisymmetric and two-dimensional, are examined to define the effect of the nozzle geometry and boundary layers on the flow. A method of defining average flow properties, which include the boundary layer influence within a one-dimensional flow formulation, is presented. The boundary layers are found to be of the same order as the nozzle exit dimensions and have a large influence on the flow. Axisymmetric and two-dimensional nozzles with the same inlet flow, geometric area ratios, and nozzle exit dimensions are found to have essentially the same average nozzle exit flow properties; the nozzle mass distributions, however, are quite different and indicate that axisymmetric nozzles may result in faster cavity mixing. Methods of including the boundary-layer influence in the laser performance and pressure recovery analyses are discussed.

Nomenclature

a = local sonic velocity
A = area
$\mathcal{A}$ = area ratio (A/A^*)
B_L = flamesheet constant, see Eq. (26)
C_p = heat capacity
$\mathfrak{D}$ = diffusion coefficient
F = nozzle axial thrust
h = enthalpy per unit mass, $\int_0^T c_p\, dT$
h_o = stagnation enthalpy per unit mass, $h + \frac{1}{2}u^2$
H_o = stagnation enthalpy flow, see Eq. (1)
ℓ = two-dimensional nozzle height
m = mass flow
M = Mach number
$\mathfrak{M}$ = momentum flow, see Eq. (1)
P = pressure
r = nozzle transverse coordinate, see Fig. 1
R = nozzle radius in subsonic region
R_u = universal gas constant
Re_o = nozzle Reynolds number, $\rho_o (2h_o)^{1/2} r^*/\mu_o$, $K_R P_{o2} r^*$
s = entropy per unit mole
T = temperature
u = velocity
V = flow speed parameter, $u^2/2h_o$
x = longitudinal wall coordinate
X_i = mole fraction
y = transverse wall coordinate
Y_i = mass fraction
z = nozzle axial coordinate
α = boundary-layer correction coefficients, see Eq. (10)
β_w = nozzle wall half-angle
γ = specific heat ratio
δ = boundary-layer thickness
δ^* = displacement thickness
η = nozzle thrust efficiency, F/F_I
θ = momentum thickness
λ = nozzle angle correction coefficient
μ = viscosity
ρ = density
σ_i = concentration thickness, ith species
ν = 0, two-dimensional nozzles; = 1, axisymmetric nozzle
ϕ = stagnation enthalpy thickness

Superscripts

$\bar{(\ )}$ = average flow quantity
$(\ )^*$ = nozzle throat

Subscripts

o = stagnation condition
2 = nozzle inlet station
3 = nozzle exit station
a = axisymmetric
$2D$ = two-dimensional
e = effective
f = flamesheet
g = geometric
i = ith species
I = inviscid
t = total
w = wall

Received Jan. 8, 1976; revision received May 3, 1976.
Index categories: Nozzle and Channel Flows; Lasers.

*Principal Scientist, High Energy Laser Technology. Member AIAA.

Introduction

In the study of chemical laser flows, the region of primary interest is in the laser optical cavity where the beam is generated. The chemical laser operates by introducing discrete fuel and oxidizer streams into the laser cavity, where they mix and react to product the vibrationally excited gas species, which form the population inversion necessary to sustain laser oscillation in the cavity.[1] In order to operate a chemical laser at high efficiency and specific power levels, one must use nozzles whose dimensions are small to promote rapid mixing of the reactants[2-7]; nozzles of both two-dimensional[2,6] and axisymmetric[6] geometries have been considered. The small nozzle dimensions result in low nozzle Reynolds numbers and nozzle flows in which the boundary layers are large. Since the laser cavity chemical reactions start at the contact point between the fuel and oxidizer streams, the initial reactions take place within the nozzle boundary layers. If the length of the lasing region is such that laser cutoff occurs before the flamesheet has moved into the nozzle core flow, then of all the reactants that contribute to the laser power originally were within the nozzle boundary layer; for this type of operation, including the boundary-layer influence in the laser cavity analysis is expected to be important. Additionally, since the nozzle boundary layers result in a reduction in the flow stagnation pressure available for recovery downstream of the laser cavity in a diffuser, the laser pressure recovery analysis should include the influence of the nozzle boundary layers.

Past studies of low Reynolds number nozzle flows have been conducted for both low-thrust-nozzle[8-10] and low-density wind-tunnel[11-15] applications. Analysis methods have

varied both in the manner in which the nozzle core flow/boundary-layer interaction was handled, and in the method used to calculate the size of the nozzle boundary layers. Rae[8] solved the Navier-Stokes equations in the channel flow approximation for the entire nozzle flowfield. All other investigators used an iterative technique to couple separate core flow and boundary-layer solutions. Murch, et al.[10] and Potter[14] used Cohen and Reshotko's[16] integral method to obtain boundary-layer solutions, whereas Whitfield[13] adopted Patanker and Spaulding's[17] numerical solution to laminar flows. Whitfield[13] has shown that inclusion of the nozzle transverse curvature effects on the boundary-layer solutions result in an increase in the size of the boundary layer in low Reynolds number axisymmetric nozzle flows. Furthermore, Whitfield[13] shows that his iterative solutions are in good agreement with the results of Rae,[8] and with the nozzle pitot probe data taken on a laser nozzle array.[18] For these reasons, Whitfield's[13] computer code was used in this study.

Past studies of laser nozzle flows by Ferrell et al.[19] and Zelazny, et al.[20] have examined the influence of nozzle design on fluorine atom recombination and the thermal-structural aspects of nozzle design, respectively. These investigations did not address the problem of including the nozzle boundary-layer influence in the laser cavity and pressure recovery analysis. Typically, the laser cavity flow is analyzed using one-dimensional streamtube models such as RESALE[21] and BLAZE-II.[22] In these models, reactant mixing is handled in a quasi two-dimensional fashion by specifying the rate at which fuel is added to the oxidizer streamtube. In order to be consistent with the one-dimensional model approximation, flow quantities used to characterize the oxidizer streamtube at the nozzle exit/laser cavity inlet station should be one-dimensional values, which are averages over the entire nozzle flow area and include the effect of the nozzle boundary layers. Herein, a method of defining one-dimensional average flow qualities, which include the influence of the nozzle boundary layers, is presented. Results of boundary-layer calculations for both nozzle geometries are presented, and the differences between nozzle core and average flow properties are illustrated. Comments are made on the inclusion of the boundary-layer influence in the laser cavity analysis.

Analysis

Whitfield's[13] computer code was the basic tool used in this study. Only laminar nozzle flows were considered. An iterative method is required to obtain a converged solution for the nozzle flow. Initial estimates for the nozzle displacement thickness were taken from the similarity solutions of Back.[23] From these estimates, an initial nozzle pressure distribution is calculated and input to the nozzle computer code. A new distribution of boundary-layer and nozzle core flow parameters is calculated and checked against those from the previous calculation. This procedure is continued until the solution has converged; solution convergence is discussed at the beginning of the following section. The flow in the nozzle core was calculated by assuming one-dimensional isentropic flow to an area corrected by the displacement thickness.

A method of calculating atomic species recombination was needed, since Ferrell et al.[19] and Zelazny et al.[20] indicate that its magnitude is significant when the nozzle wall is catalytic. If one examines the transformed boundary-layer equations given by Fay and Riddell[24] under the restrictions of negligible gas phase recombination, unity Prandtl and Lewis numbers, and viscosity proportional to temperature (conditions approximately true in laser nozzle flows), then the species and energy equations are identical, and have identical boundary conditions when the dependent variables are G and S_i, where $G=(h_o-h_w)/(h_{o3}-h_w)$ and $S_i=(Y_i-Y_{wi})/(Y_{3i}-Y_{wi})$. Herein, the species distributions across the boundary layer were obtained by setting $S_i=G$; wall catalicity can be varied by changing Y_{wi}.

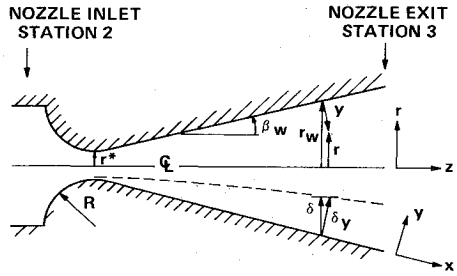

Fig. 1 Nozzle geometry.

In the remainder of this section, the defining equation for the boundary-layer integral parameters and one-dimensional average flow quantities are derived. The integral parameters are derived in terms of an area rather than a linear dimension, e.g., displacement area rather than thickness, since this allows one to handle axisymmetric and two-dimensional nozzle flows within a uniform formulation. The nozzle geometry is shown in Fig. 1. Wall coordinates in which the boundary-layer problem is solved are (x,y); nozzle coordinates are (z,r). The mass, momentum, and stagnation enthalpy flow through the nozzle exit control surface are given in Eq. (1). A planar control surface is used, and the correction for divergence angle, given by Landsbaum,[25] is neglected since it is small for the wall angles used in laser nozzles.

$$m=\int_{c.s}\rho u dA \qquad \mathfrak{M}=\int_{c.s}u\rho u dA \qquad H_o=\int_{c.s}h_o\rho u dA \tag{1}$$

In the r coordinate, the area elements for the two-dimensional and axisymmetric nozzles are $dA=2\ell dr$ and $dA=2\pi r dr$, respectively. Define geometric constants $K_g=2\ell$ and $\nu=0$ for two-dimensional nozzles and $K_g=2\pi r_w$ and $\nu=1$ for axisymmetric nozzles. Additionally, write $\hat{r}=r/r_w=[1-(y\cos\beta_w/r_w)]$. With $dr=-dy\cos\beta_w$, the area element in the y coordinate can be written as $dA_y=-K_g\hat{r}^\nu\cos\beta_w dy$ for both nozzle geometries. The area element is required in the y coordinate since $\rho=\rho(y)$ and $u=u(y)$, as obtained from the boundary-layer solutions.

In order to evaluate Eq. (1) for the nozzle mass flow, the integral is evaluated separately over the nozzle core flow and boundary layer. The flow is uniform in the nozzle core, with $\rho u=\rho_3 u_3$. Equation (1) then can be written as shown in Eq. (2), where $\delta=\delta_y\cos\beta_w$.

$$m=\int_0^{r_w-\delta}\rho u dA+\int_{r_w-\delta}^{r_w}\rho u dA=\rho_3 u_3\int_0^{r_w}dA + \int_{r_w}^{r_w-\delta}(\rho_3 u_3-\rho u)dA \tag{2}$$

The integral of dA over the interval $0\rightarrow r_w$ is A_g, the geometric flow area. Writing the last integral in the y coordinate, the mass flow is then given by Eq. (3). The last term in Eq. (3) is an area correction due to nozzle boundary layers.

$$m=\rho_3 u_3\left[A_g-K_g\cos\beta_w\int_0^{\delta_y}\left(1-\frac{\rho u}{\rho_3 u_3}\right)\hat{r}^\nu dy\right] \tag{3}$$

The integral reduces to the standard textbook definition for the displacement thickness when the nozzle is two-dimensional ($\upsilon=0$), or when transverse curvature effects are negligible ($\delta_y/r_w\ll 1$). Defining a displacement area as shown in Eq. (4), we can write the nozzle mass flow as indicated in Eq. (5), where A_e, is the effective flow area, which describes the nozzle mass flow in terms of the freestream mass flux; A_{δ^*} is related to δ^* by Eq. (6). Since δ^* represents the displacement of the wall required to describe the nozzle mass flow in terms

of the core flow mass flux, $A_{\delta}{}^{*}$ represents the area displayed by moving the wall a distance δ^{*}.

$$A_{\delta^{*}} = K_g \cos\beta_w \int_0^{\delta_y} \left(1 - \frac{\rho u}{\rho_3 u_3}\right)\left[1 - \frac{y\cos\beta_w}{r_w}\right]^{v} dy \tag{4}$$

$$m = \rho_3 u_3 (A_g - A_{\delta^{*}}) = \rho_3 u_3 A_e \tag{5}$$

$$A_{\delta^{*}}/A_g = \delta^{*}/r_w (2 - \delta^{*}/r_w)^{v} \tag{6}$$

As in the case of Eq. (5) for the mass flow, equations can be written to describe the flow of momentum and stagnation enthalpy in terms of core flow properties, the geometric area, and an area correction for the boundary layer. The derivation is in terms of a general specific quantity f, which represents the velocity u in the momentum equation, the stagnation enthalpy h_o in the energy equation, and the i^{th} species mass fraction Y_i in the species equation. A general boundary-layer thickness ϵ and area A_{ϵ} are used, where $\epsilon = \theta, \phi$, and σ_i in the momentum, energy, and species equations, respectively. The derivation is similar to that previously given, and Eq. (7) corresponds to Eq. (3).

$$F = \rho_3 u_3 f_3 \left[A_g - K_g \cos\beta_w \int_0^{\delta_y} \left(1 - \frac{\rho u}{\rho_3 u_3}\right) \hat{r}^{v} dy - K_g \cos\beta_w \int_0^{\delta_y} \frac{\rho u}{\rho_3 u_3} \left(1 - \frac{f}{f_3}\right) \hat{r}^{v} dy\right] \tag{7}$$

The first term in brackets is the geometric flow area, the second is $A_{\delta^{*}}$, and the third is the correction A_{ϵ}, where A_{ϵ} is defined as shown in Eq. (8). The relationship between ϵ and A_{ϵ} is the same as that given in Eq. (6) for δ^{*} and $A_{\delta^{*}}$. By use of Eq. (5) for the mass flow, Eq. (7) can be written as shown in Eq. (9).

$$A_{\epsilon} = K_g \cos\beta_w \int_0^{\delta_y} \frac{\rho u}{\rho_3 u_3} \left(1 - \frac{f}{f_3}\right)\left[1 - \frac{y\cos\beta_w}{r_w}\right]^{v} dy \tag{8}$$

$$F = \rho_3 u_3 f_3 (A_g - A_{\delta^{*}} - A_{\epsilon}) = m f_3 (1 - A_{\epsilon}/A_e) \tag{9}$$

The factor $(1 - A_{\epsilon}/A_e)$ describes the loss of momentum, stagnation enthalpy, and the i^{th} species due to the nozzle boundary layers. Note that A_{ϵ} can be zero, even when the nozzle boundary layers are large, e.g., in an adiabatic nozzle flow. If we define correction factors

$$\alpha_1 = 1 - A_{\delta^{*}}/A_g \qquad \alpha_2 = 1 - A_{\theta}/A_e$$
$$\alpha_3 = 1 - A_{\phi}/A_e \qquad \alpha_{4i} = 1 - A_{\sigma i}/A_e \tag{10}$$

then the mass, momentum, stagnation enthalpy, and i^{th} species mass flow through the nozzle control surface can be written as shown in Eq. (11).

$$m = \rho_3 u_3 A_g \alpha_1 \qquad \mathfrak{M} = m u_3 \alpha_2$$
$$\mathrm{H}_o = m h_{o3} \alpha_3 \qquad m_i = m Y_{3i} \alpha_{4i} \tag{11}$$

One-dimensional average flow quantities now are derived for a thermally perfect gas; the flow is assumed to be uniform over the geometric flow areas. Average flow properties are denoted by an overbar. The average velocity, stagnation enthalpy, and i^{th} species mass fraction can be written from Eq. (11) as shown in Eq. (12).

$$\bar{u} = \alpha_2 u_3 \qquad \bar{h}_{o3} = \alpha_3 h_{o3} \qquad \bar{Y}_{3i} = \alpha_{4i} Y_{3i} \tag{12}$$

The average static enthalpy is derived from the one-dimensional energy equation as indicated in Eq. (13):

$$\bar{h}_3 = \bar{h}_{o3} - \tfrac{1}{2}\bar{u}_3^2 = h_{o3}[\alpha_3 - \alpha_2^2 V] \tag{13}$$

The mass average gas density is obtained from the continuity equation, as shown in Eq. (14).

$$m = \rho_3 u_3 A_g \alpha_1 = \bar{\rho}_3 \bar{u}_3 A_g, \quad \bar{\rho}_3 = (\alpha_1/\alpha_2)\rho_3 \tag{14}$$

Defining an average Mach number as $\bar{M}_3 = \bar{u}_3/\bar{a}_3$, we can relate $\bar{M}_3$ to M_3 as shown in Eq. (15).

$$\bar{M}_3^2 = \alpha_2^2 [\gamma(T_3)/\gamma(\bar{T}_3)] (T_3/\bar{T}_3) M_3^2 \tag{15}$$

The average temperature $\bar{T}_3$ is assumed to be known from Eq. (13). The gas static pressure P_3 is that imposed on the flow from the nozzle core flow solutions. It is obtained by calculating the flow expansion to an area corrected by $A_{\delta^{*}}$. If the average flow quantities are to have the same mass, momentum, and stagnation enthalpy flow as the actual nozzle, i.e., Eq. (11) is to be satisfied, then it is necessary to calculate an average static pressure $\bar{P}_3$ from the perfect gas relation as shown in Eq. (16).

$$\bar{P}_3/P_3 = \bar{\rho}_3 \bar{T}_3/\rho_3 T_3 = (\alpha_1/\alpha_2)(\bar{T}_3/T_3) \tag{16}$$

The ratio $\bar{P}_3/P_3$ represents the second-order correction to the gas pressure due to the momentum and energy losses in the nozzle; $A_{\delta^{*}}/A_g$ is the first-order correction.

In general, laser nozzle flows cannot be considered to be calorically perfect because of the presence of polyatomic gas species in the flow and the large static temperature difference between nozzle inlet and exit; the temperatures T_{o3} and T_3 therefore must be calculated by evaluating the enthalpy integrals. If, however, we consider the flow to be calorically perfected over a restricted temperature range, we can evaluate these quantities analytically. In the region about T_{o3}, let the gas heat capacity and specific heat ratio be C_{po} and γ_o, respectively; in the region about T_3, they are C_{p3} and γ_3, respectively. Then $\bar{T}_{o3}$ and $\bar{T}_3$ can be written as shown in Eqs. (17) and (18). If the gas is calorically perfect over the entire temperature range, then $C_{po} = C_{p3}$ and $\gamma_o = \gamma_3$.

$$\bar{T}_{o3} = T_{o3} - (1 - \alpha_3)(h_{o3}/C_{po}) \tag{17}$$

$$\bar{T}_3 = T_3 + [V(1 - \alpha_2^2) - (1 - \alpha_3)](h_{o3}/C_{p3}) \tag{18}$$

As yet undefined is the average stagnation pressure of the gas at the nozzle exit P_{o3}. This is the pressure that would exist if the nozzle exit flow were decelerated isentropically. The entropy of a gas mixture is given by Eq. (19). If we form the entropy difference between any two states, a and b, assume that the process between the two states is isentropic and that the gas composition is chemically frozen during the process, then the pressures and temperatures of states a and b are related as indicated in Eq. (20).

$$\frac{1}{R_u} s = \int_0^T \frac{C_p(T)}{R_u} \frac{dT}{T} - \ln P - \sum_i X_i \ln X_i \tag{19}$$

$$\frac{P_b}{P_a} = \exp[\Psi(T_b) - \Psi(T_a)] \qquad \Psi(T) = \int_0^T \frac{C_p(T)}{R_u} \frac{dT}{T} \tag{20}$$

This equation relates (P_{o2}, T_{o2}) to (P_3, T_3), and $(\bar{P}_{o3}, \bar{T}_{o3})$to $(\bar{P}_3, \bar{T}_3)$. If we form the ratio $\bar{P}_{o3}/P_{o2}$, we can write the reduction in the nozzle stagnation pressure as shown in Eq. (21) for a thermally perfect gas, as shown in Eq. (22) if the gas is assumed to be calorically perfect over a limited temperature range, and as shown in Eq. (23) for a calorically perfect gas. Note that, when the specific heat ratio is constant, the average static and stagnation pressures are related to the average Mach number by the normal one-dimensional relationship

$$\bar{P}_{o3}/P_{o2} = (\bar{P}_3/P_3)\exp\{[\Psi(\bar{T}_{o3}) - \Psi(T_{o3})] - [\Psi(\bar{T}_3) - \Psi(T_3)]\} \tag{21}$$

$$\frac{\bar{P}_{o3}}{P_{o2}} = \frac{\bar{P}_3}{P_3}\left(\frac{\bar{T}_{o3}}{T_{o3}}\right)^{\gamma_o/(\gamma_o-1)}\left(\frac{T_3}{\bar{T}_3}\right)^{\gamma_3/(\gamma_3-1)} \quad (22)$$

$$\frac{\bar{P}_{o3}}{P_{o2}} = \frac{\bar{P}_3}{P_3}\left[\frac{1+[(\gamma-1)/2]\bar{M}_3^2}{1+[(\gamma-1)/2]M_3^2}\right]^{\gamma/(\gamma-1)} \quad (23)$$

The average nozzle exit flow parameters form a consistent set, which satisfy the one-dimensional flow equations. The were derived so that they result in the same nozzle exit mass, momentum, and stagnation enthalpy flow as that from the actual nozzle with nonuniform exit flow conditions. The difference between the nozzle exit core and average flow properties can be viewed as the differences between two thermodynamic states. The average flow quantities represent a higher entropy level state because of the nozzle viscous losses, which are defined by the quantities α_1, α_2, and α_3; these quantities essentially represent the thermodynamic path between the two states (P_{o2},h_{o2}) and $(\bar{P}_{o3},\bar{h}_{o3})$.

Results and Discussion

Analysis Verification

For all of the results presented herein, the nozzle had the geometry shown in Fig. 1, with $R=3r^*$ for all calculations. Fixed computational variables were the step size at 7.5% of the local wall radius, the number of transverse locations across the boundary layer at 50, and the location of the boundary layer at the point where the velocity was 99.5% of the core flow value. Since the flow solution is obtained through an iterative process, a convergence criterion was required to indicate a valid solution. For this study, convergence was formulated in terms of the core Mach number M_3. The solution was assumed to have converged when the difference in M_3 from successive iterations was less than 0.05. Figure 2 shows the approach to convergence for a typical case; seven iterations were required. When this solution had converged, the variation in the displacement thickness was less than 1.0% for successive iterations. It was found that the number of iterations required for convergence increased as the Reynolds number decreased and the nozzle area ratio increased. For this study, a maximum of nine iterations was used to obtain a solution. In general, it required about 30 sec of computer time per iteration on the IBM 360-70 computer.

Before proceeding to the study of laser nozzle flows, it was thought necessary to compare the analysis with data. The average flow properties are not themselves measurable quantities; however, the nozzle thrust can be written in terms of the average flow properties, and thrust measurements in low Reynolds number nozzle flows are available for comparison. From Landsbaum,[25] the thrust of a conical nozzle with a calorically perfect gas can be written in terms of average flow properties, as shown in Eq. (24): λ is the correction factor to account for the nonaxial velocity component at the nozzle exit; $\bar{M}_3$ is the average Mach number from Eq. (15); $\bar{P}_3/P_3$ is the second-order pressure correction from Eq. (16); and P_3/P_{o2} is the nozzle pressure ratio obtained by correcting the nozzle by A_{δ^*} and expanding it to M_3. The thrust of the ideal inviscid nozzle is obtained by allowing the flow to expand to the geometric area ratio with no viscous loss. The nozzle exit Mach number is M_{3g}, and the nozzle pressure ratio is P_{3g}/P_{o2}; the nozzle thrust is given by Eq. (25), and the nozzle thrust efficiency is given by $\eta = F/F_I$

$$F = \lambda m\bar{u}_3 + \bar{P}_3 A_g = P_{o2}A_g(\bar{P}_3/P_3)(P_3/P_{o2})(1+\lambda\gamma\bar{M}_3^2) \quad (24)$$

$$F_I = mu_{3g} + P_{3g}A_g = P_{o2}A_g(P_{3g}/P_{o2})(1+\gamma M_{3g}^2) \quad (25)$$

The data of Murch et al.[10] were compared with the results from the present analysis. The data selected for comparison were those for the 20° conical nozzle with a geometric area ratio of 20, using 1500°F hydrogen propellant (see Fig. 5 of Murch et al.[10]). The test data and the results from this analysis are shown in Fig. 3. Over most of the Reynolds number range, the present theory is within 2.0% of the experimental data. For the calculation, λ was set equal to unity, since most of the nozzle mass flow is near the centerline. For a uniform mass distribution across the nozzle, Landsbaum's equation would give $\lambda = 0.97$; therefore, setting $\lambda = 1$ gives a slightly optimistic prediction. For the theoretical calculation shown in Fig. 3, the wall temperature was constant at 40% of the core flow stagnation temperature. The second-order correction, $\bar{P}_3/P_3$ is significant for this calculation, varying from about 0.85 to 0.90. The average flow properties, $\bar{M}_3, \bar{P}_{o3}$, and $\bar{T}_3$ are also significantly different from those in the core flow and, therefore, provide a good test of their usefulness. Since Eq. (24) does provide an accurate estimate of the nozzle efficiency and shows the correct performance trend, it is thought that the average flow properties are meaningful quantities.

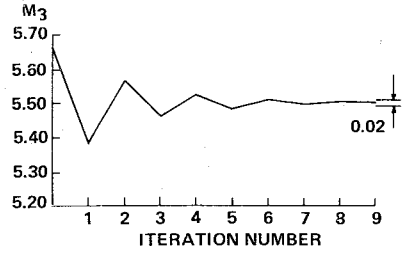

Fig. 2 Solution convergence for a two-dimensional nozzle, $Re_o = 1000$. $\mathcal{R}_g = 39, \beta_w = 15°$.

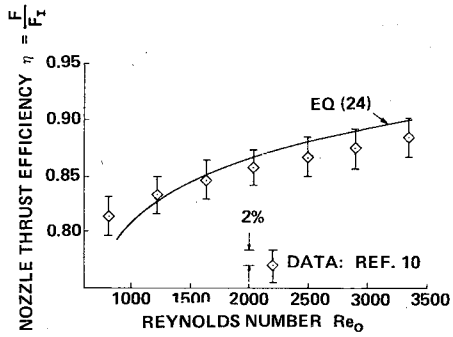

Fig. 3 Nozzle thrust efficiency: Comparison of theory with data.

Boundary-Layer Calculations

Both two-dimensional and axisymmetric laser nozzles were examined for geometric area ratios as large as 40. Nozzle wall half-angles were varied in the range of 10° to 20°, nozzle Reynolds numbers in the range of $4\text{-}100\times10^2$ for two-dimensional nozzles, and $1\text{-}40\times10^3$ for axisymmetric nozzles. The wall temperature boundary condition was the same for all calculations. In the subsonic nozzle region, the wall temperature was 60% of the gas stagnation temperature; in the supersonic region, the wall temperature decreased linearly with distance from 60% of the gas stagnation temperature at the throat to 30% at the nozzle exit ($\mathcal{R}_g = 40$). Gas properties assumed constant for all calculations were the Prandtl number at 0.54 and the temperature viscosity exponent ($\mu \sim T^\omega$) at 0.67. The gas specific heat ratio was varied from 1.58 to 1.38, with the nominal value being 1.58.

Figure 4 shows the result of a typical calculation for a 15° two-dimensional nozzle at a Reynolds number of 600. The nozzle Reynolds number can be written as $Re_o = K_R P_{o2} r^*$ where K_R is a constant dependent on the gas stagnation temperature and composition. For a chemical laser with $T_{o2} = 1600°$K, a typical value of K_R is 5000 (lbf/in.)$^{-1}$. For two-dimensional chemical laser nozzles, a typical value for r^* is about 0.005 cm or 0.002 in., resulting in $P_{o2} = 60$ psia for Re_o

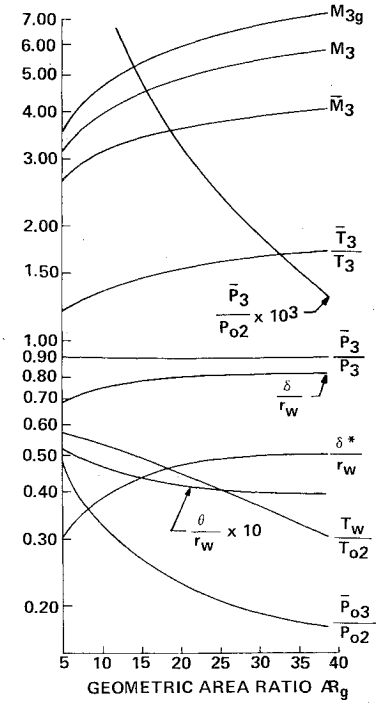

Fig. 4 Nozzle exit flow properties, two-dimensional, $Re_o = 600$, $\beta_w = 15°$, $\gamma = 1.58$.

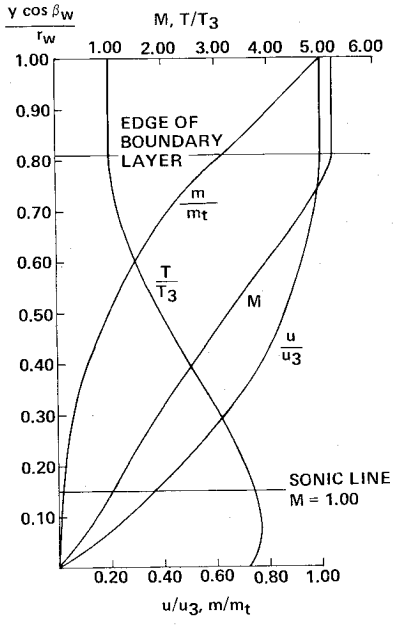

Fig. 5 Mass flow, velocity, Mach number, and static temperature distributions across two-dimensional nozzle, $Re_o = 600$, $AR_g = 25.7$, $\beta_w = 15°$, $\gamma = 1.58$.

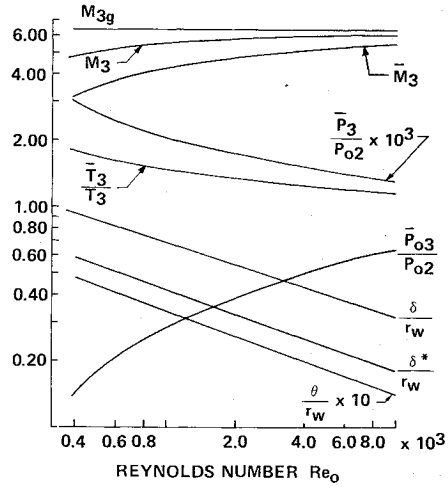

Fig. 6 Nozzle exit flow properties, two-dimensional, $A\!R_g = 25$, $\beta_w = 15°$, $\gamma = 1.58$.

$= 600$. With these values, the nozzle exit pressure P_3 is in the range of 4-15 Torr, depending on the nozzle area ratio.

For two-dimensional flows, $\delta^*/r_w = A_{\delta^*}/A_g$; the results in Fig. 4 therefore are shown in terms of the boundary-layer thickness rather than area. At this low Reynolds number, the boundary layers are large, covering 69-82% of the nozzle flow area. This displacement thickness δ^*/r_w varies from 30 to 50% of the nozzle geometric area, indicating that the effective nozzle area is substantially less than the geometric area ratio. The momentum thickness is 4-5%, and the energy thickness was of the same order. The nozzle wall temperature distribution T_w/T_{o2}, used in this calculation, also is shown.

Three Mach numbers are shown in Fig. 4: M_{3g}, the inviscid flow Mach number; M_3, the core flow value; and $\bar{M}_3$, the average value. At $A\!R_g = 25$, $M_{3g} = 6.35$, $M_3 = 5.15$, and $\bar{M}_3 = 4.75$; $\bar{M}_3$ is lower than M_3, since the average flow velocity is lower and the static temperature higher than that in the nozzle core, i.e., $\bar{u}_3/u_3 = 0.92$ while $\bar{T}_3/T_3 = 1.60$. The average stagnation pressure $\bar{P}_{o3}$ declines rapidly as the nozzle area ratio increases, having a value only 21% of that in the core flow at $A\!R_g = 25$. The second-order pressure correction $\bar{P}_3/P_3$ is relatively constant at a value of 0.89, and it differs sufficiently from unity that it cannot be neglected; $\bar{P}_3/P_{o2}$ gives the nozzle static/stagnation pressure ratio. For the conditions shown in Fig. 4 at $A\!R_g = 25$, a nozzle wall fully catalytic to atom recombination would reduce the atomic specie mass fraction by 10%, i.e., $\bar{Y}_{3i}/Y_{3i} = 0.90$. This result is estimated from the energy thickness, as discussed in the previous section, and is in agreement with the values given by Zelazny et al.[20]

The nozzle mass flow, velocity, static temperature, and Mach number distributions are shown in Fig. 5 for $A\!R_g = 25.7$. Over most of the nozzle, the static temperature is significantly larger than the core flow temperature; for this reason, the average static $\bar{T}_3$ is 60% greater than T_3. Since the static temperature is relatively high in the near wall region, the gas density and mass flux are correspondingly low. This results in most of the nozzle mass flow being in the region near the nozzle centerline. About 2% of the nozzle mass flow is in the nozzle subsonic region, which covers about 15% of the geometric flow area. In the near wall region, 20% of the mass flow occupies 50% of the flow area; 60% of the nozzle flow is within the boundary layer.

The influence of the nozzle Reynolds number on the nozzle boundary-layer thicknesses, core, and average flow properties is shown in Fig. 6. Increasing the Reynolds number corresponds to increasing the upstream stagnation pressure P_{o2}, or throat width r^*, for a constant gas stagnation temperature and composition. The nozzle flow becomes fully viscous when the Reynolds number is about 300; as the nozzle Reynolds number increases, the boundary-layer thicknesses decreases. In the Reynolds number range of 500-2000, which is the range of interest for two-dimensional laser nozzles, the variation in the average flow parameters is significant, e.g., as Re_o increases from 500 to 2000, $\bar{P}_{o3}$ more than doubles, $\bar{M}_3$ increases from 3.45 to 4.70, $\bar{T}_3$ decreases from 1.65 to 1.33, and $\bar{P}_3/P_{o2}$ decreases from 2.6×10^{-3} to 1.72×10^{-3}.

The influence of the nozzle wall angle, wall temperature, and gas specific heat ratio on the displacement thickness was found to be relatively small. For the $A\!R_g = 25$ nozzle, increasing β_w from 15° to 20°, reducing T_w/T_{o2} from 0.40 to 0.20, or decreasing γ from 1.58 to 1.38, each resulted in a reduction of δ^*/r_w by about 20%.

Boundary-layer calculations made for axisymmetric nozzles show the same performance trends as did the two-dimensional nozzles; the axisymmetric nozzles, however, become fully viscous at Reynolds number on the order of 1000. For a 15° axisymmetric nozzle in the range $5 \le A\!R_g \le 40$ with $Re_o = 3000$, the boundary layer, i.e., A_δ/A_g, covers from 65 to 85% of the

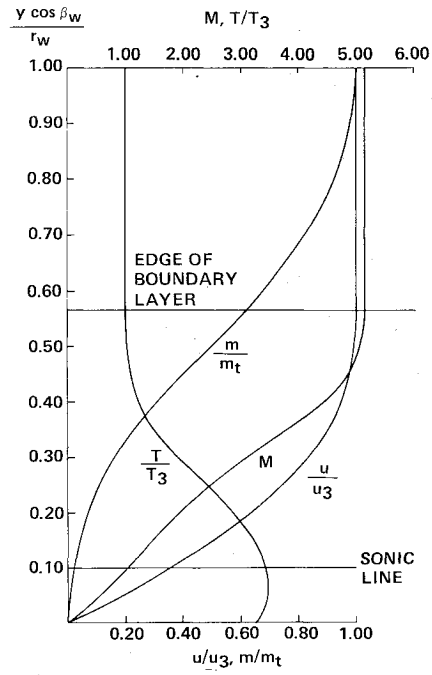

Fig. 7 Mass flow, velocity, Mach number, and static temperature distributions across axisymmetric nozzle, $Re_o = 3000$, $\mathcal{R}_g = 25.5$, $\beta_w = 15°$, $\gamma = 1.58$.

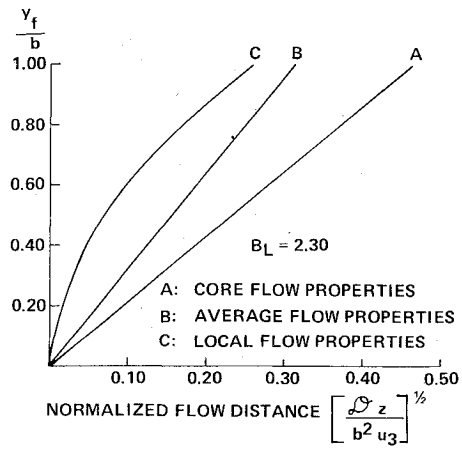

Fig. 8 Flamesheet penetration for core, average, and local nozzle exit flow properties: two-dimensional nozzle.

geometric flow area. The area displacement, i.e., A_{δ^*}/A_g varies from 26 to 52%. The displacement thickness δ^*/r_w, related to A_{δ^*}/A_g through Eq. (6), varies from 14 to 32%.

If we compare the flows in two-dimensional and axisymmetric nozzles for the same nozzle inlet flow, i.e., K_R and P_{o2} are constant, then differences in the nozzle Reynolds numbers will be solely due to difference in the throat dimension r^*. For two-dimensional nozzles, the geometric relationship between the geometric area ratio, nozzle inlet and exit dimensions is $r_{w,2D} = \mathcal{R}_g r^*_{2D}$; for axisymmetric nozzles, it is $r_{w,a} = \mathcal{R}_g^{1/2} r^*_a$. Therefore, it is not possible to have all three quantities equal for the two nozzle geometries. If we compare flows for equal Reynolds numbers, i.e., $r^*_a = r^*_{2D}$, and equal geometric area ratios, then the axisymmetric nozzle is found to be the more viscous of the two. On the basis, however, the axisymmetric nozzle would be expected to have a superior laser efficiency, since its exit dimension is smaller by a factor of $\mathcal{R}_g^{1/2}$ than that of the two-dimensional nozzle.

A better comparison of the two nozzle geometries is obtained on the basis of equal geometric area ratios and nozzle exit dimensions, since the nozzle exit dimension is a critical parameter in defining the mixing length scale in the laser performance analysis.[2-5,7] The nozzle throat dimensions are then related by $r^*_a = \mathcal{R}_g^{1/2} r^*_{2D}$, and the Reynolds numbers by

$$Re_{o,a} = \mathcal{R}_g^{1/2} Re_{o,2D}$$

When $\bar{P}_3$, $\bar{M}_3$, and $\bar{P}_{o3}$ were compared for the two nozzle geometries over the area ratio range of $5 \le \mathcal{R}_g \le 40$, it was found that these parameters varied by less than 10% due to geometric differences. Therefore, in terms of the average nozzle exit flow properties, axisymmetric and two-dimensional nozzles will have about the same nozzle exit flow when the nozzle inlet flow is the same, the geometric area ratios and nozzle exit dimensions are equal, and $Re_{o,a} = \mathcal{R}_g^{1/2} Re_{o,2D}$.

Nozzle mass flow, velocity, static temperature, and Mach number distributions are shown in Fig. 7 for a 15° axisymmetric nozzle with $\mathcal{R}_g = 25.5$ and $Re_o = 3000$. The average flow properties for this nozzle flow are the same as those for the 15° two-dimensional nozzle, with $Re_o = 600$ shown in Fig. 5. Although the area terms A_δ/A_g, A_{δ^*}/A_g, etc., are about the same for both nozzles, the linear dimensions δ/r_w, δ^*/r_w, etc., are not equal, and are smaller in the axisymmetric nozzle. Perhaps the most notable difference between the two is that the axisymmetric nozzle has a greater percentage of its mass flow in the near-wall region than does the two-dimensional nozzle, e.g., the axisymmetric nozzle has about 50% of its mass flow in the region $0 \le y\cos\beta_w/r_w \le 0.50$, whereas two-dimensional nozzle has only 20%. Both nozzles have about 60% of the mass flow within the boundary layer.

Laser Performance Implications

The flamesheet models of laser flows[3-5,7] indicate that lasing performance is sensitive to the fuel and oxidizer mixing rate. Mirels et al.[3] used Eq. (26) to describe the flamesheet location

$$y_f/b = B_L [\mathcal{D}z/b^2 u]^{1/2} \tag{26}$$

for two-dimensional flows with laminar mixing, where $\mathcal{D}$ is the diffusion coefficient, b the nozzle exit half-width, z the distance from the nozzle exit, u the flow velocity, and B_L a mixing constant with a value of about 2.30. Equation (26) is valid for uniform nozzle flows; for nonuniform flows, a differential form is used to describe the influence of the local flow properties on y_f. Figure 8 shows the flamesheet penetration of the nozzle flow shown in Fig. 5 based on the core, average, and local flow properties. The implication of Fig. 8 is that the flamesheet location is a function of the nozzle boundary layers, and that an accurate description of y_f requires the use of the boundary-layer profiles.

The flamesheet location, however, is important only as it affects the rate at which the nozzle mass flow enters the reaction zone. For two-dimensional nozzles with uniform flow properties, either core values or average, the fraction of the nozzle mass flow, which has intercepted the flamesheet, i.e., m_f/m_t, is equal to y_f/b. The distribution of m_f/m_t based on the boundary-layer profiles can be found from the results given in Figs. 5 and 8. The results in terms of m_f/m_t are shown in Fig. 9 and indicate that use of average flow properties yields about the same mixing rate as do the boundary-layer profiles, whereas use of core flow properties gives too slow a mixing rate. Therefore, to a first order, it is thought that the average flow properties describe the boundary-layer influence on the laminar mixing rate.

In comparing the two-dimensional nozzle flow of Fig. 5, and the axisymmetric flow of Fig. 7, it is noted that although both have the same average nozzle exit flow properties, i.e., $\bar{M}$, $\bar{T}$, etc., the boundary-layer profiles are quite different. In terms of mass distribution, m/m_t, the axisymmetric nozzle has a greater fraction of its mass flow in the near-wall region than does the two-dimensional nozzle. Assuming that the flamesheets for the two nozzle geometries are not very dif-

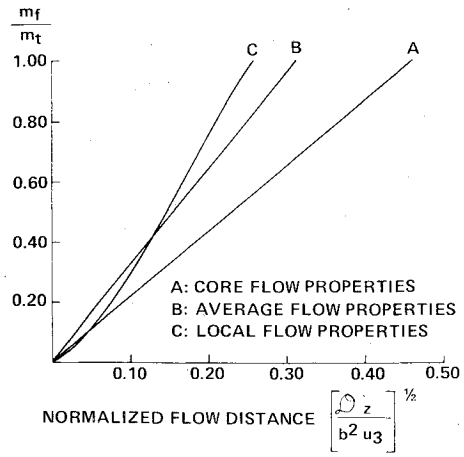

Fig. 9 Mass flow intercepted by flamesheet for core, average, and local nozzle exit flow properties: two-dimensional nozzle.

ferent in the near-wall region, the mass distributions would indicate that, for any flamesheet penetration, the axisymmetric nozzle would place a larger fraction of its mass flow in the reaction zone than would the two-dimensional nozzle, i.e., it would mix the reactants faster. Since the analytical models indicate that faster mixing improves the laser performance, it is thought that a laser using axisymmetric nozzles would have a higher efficiency than one that used a comparable two-dimensional nozzle, and such an improvement has been observed experimentally.[6]

The calculation of lasing performance parameters, using either analytical[3-5,7] or computer[21,22] models, is a complex task, which requires accurate descriptions for the mixing and kinetic rates that govern the production and destruction of the lasing species. These rate processes are temperature-dependent in a complex manner, and since there can be large static temperature variations across the nozzle as indicated in Figs. 5 and 7, it probably is inadequate to characterize them by a single temperature, either core value or average. In particular, for a laser operating in the mixing limited regime, where lasing ceases before the flow is fully mixed, the characteristic lasing temperature may be closer to the wall value than to the core or average temperature, and use of the latter values could lead to large errors. Therefore, it is thought that, in determining laser performance, it is necessary to use the boundary-layer profiles to characterize the flow, and a method by which this can be done within the framework of the one-dimensional flow models is given in Ref. 22.

Laser pressure recovery, on the other hand, depends more on the global flow properties than on the cavity rate processes, e.g., the magnitude of the heat release rather than the rate at which the flow is heated. Since the average flow properties adequately describe the influence of the nozzle boundary layers on the flow as a whole, it is thought that their use in the pressure recovery analysis is appropriate, and their use in this context is illustrated in Ref. 26.

Conclusions

Chemical laser nozzle flows were found to be highly viscous with boundary layers of the same order as the nozzle dimensions. Average flow properties that include the boundary-layer influence are significantly different from the nozzle core flow properties. Average properties provide a first-order description of the boundary-layer influence on the cavity flow, and are thought to be appropriate in the laser pressure recovery analysis. In the study of lasing phenomena, however, it is thought necessary to use the boundary-layer profiles to characterize the nozzle exit flow due to the large static temperature variations across the nozzle and the influence this can have on the lasing rate processes. Differences in the mass distributions across axisymmetric, and two-dimensional nozzles with the same average flow properties indicate a potential for increased laser peformance with axisymmetric nozzles; this should be given further study.

References

[1]Warren, W. R., "Chemical Lasers," *Astronautics and Aeronautics*, Vol. 13, April 1975, pp. 36-49.

[2]Mirels, H. and Spencer, D. J., "Power and Efficiency of a Continuous HF Chemical Laser," *IEEE Journal of Quantum Electronics*, Vol. QE-7, 1971, pp. 501-507.

[3]Mirels, H., Hofland, R., and King, W. S., "Simplified Model of CW Diffusion-Type Chemical Laser," *AIAA Journal*, Vol. 11, Feb. 1973, pp. 156-164.

[4]Hofland, R. and Mirels, H., "Flamesheet Analysis of CW Diffusion-Type Chemical Lasers, I., Uncoupled Radiation," *AIAA Journal*, Vol. 10, April 1972, pp. 420-428.

[5]Hofland, R. and Mirels, H., "Flamesheet Analysis of CW Diffusion-Type Chemical Lasers, II., Coupled Radiation," *AIAA Journal*, Vol. 10, Oct. 1972, pp. 1271-1280.

[6]Durran, D. A. and Spencer, D. J., "Axisymmetric Mixing Nozzle for Supersonic Diffusion Laser," The Aerospace Corp., TOR-0059(6756-02)-1, July 1970.

[7]Broadwell, J. E., "Effect of Mixing Rate on HF Chemical Laser Performance," *Applied Optics*, Vol. 13, April 1974, pp. 962-967.

[8]Rae, W. J., "Some Numerical Results on Viscous Low-Density Nozzle Flows in the Slender-Channel Approximation," *AIAA Journal*, Vol. 9, May 1971, pp. 811-820.

[9]Rothe, D. E., "Electron Beam Studies of viscous Flow in Supersonic Nozzles," *AIAA Journal*, Vol. 9, May 1971, pp. 804-811.

[10]Murch, C. K., Broadwell, J. E., Silver, A. H., and Marcisy, T. J., "Performance Losses in Low-Reynolds Number Nozzles," *Journal of Spacecraft and Rockets*, Vol. 5, Sept. 1968, pp. 1090-1094.

[11]Whitfield, D. L., "Theoretical and Experimental Investigation of Boundary Layers in Low-Density Hypersonic Axisymmetric Nozzles," Arnold Engineering Development Center, TR-68-183, 1968.

[12]Whitfield, D. L. and Lewis, C. H., "Boundary-Layer Analysis of Low-Density Nozzles, Including Displacement, Slip, and Transverse Curvature," *Journal of Spacecraft and Rockets*, Vol. 7, April 1970, pp. 462-468.

[13]Whitfield, D. L., "Viscous Effects in Low-Density Nozzle Flows," Arnold Engineering Development Center, TR-73-52, 1973.

[14]Potter, J. L. and Carden, W. H., "Design of Axisymmetric Contoured Nozzles for Laminar Hypersonic Flow," *Journal of Spacecraft and Rockets*, Vol. 5, Sept. 1968, pp. 1095-1100.

[15]Carden, W. H., "Local Heat-Transfer Coefficients in a Nozzle with High-Speed Laminar Flow," *AIAA Journal*, Vol. 3, Dec. 1965, pp. 2183-2188.

[16]Cohen, C. B. and Reshotko, E., "The Compressible Laminar Boundary Layer with Heat Transfer and Arbitrary Pressure Gradient," NACA Rept. 1294, 1956.

[17]Patanker, S. V. and Spaulding, D. B., *Heat and Mass Transfer in Boundary Layers*, 2nd ed., Intertext Books, London, 1967.

[18]Whitfield, D. L., Lewis, J. W. L., and Williams, W. D., "Specie Number Density, Pitot Pressure, and Flow Visualization in the Near Field of Two Supersonic Nozzle Banks Used for Chemical Laser Systems," AIAA Paper 73-642, 1973.

[19]Ferrell, J. E., Kendall, R. M., and Tong, H., "Recombination Effects in Chemical Laser Nozzles," AIAA Paper 73-643, 1973.

[20]Zelazny, S. W., Manhardt, P. D., and Baker, A. J., "Fluid-Thermal-Structural Analysis of Chemical Laser," AIAA Paper 74-1140, 1974.

[21]Emanuel, G., Adams, W. D., and Turner, E. B., "RESALE-1: A Chemical Laser Computer Program," Aerospace Corporation TR-0172-(2276)-1, March 1972.

[22]Zelazny, S.W., Driscoll, R.J., Raymonda, J.W., Blauer, J.A., and Solomon, W.C., "Modeling DF/HF CW Lasers: An Examination of Key Assumptions," submitted to AIAA 15th Aerospace Sciences Meeting.

[23]Back, L.H., "Acceleration and Cooling Effects in Laminar Boundary Layers-Subsonic, Transonic, and Supersonic Speeds,"

[24]Fay, J. A. and Riddell, F. R., "Theory of Stagnation Point Heat Transfer in Dissociated Air," *Journal of the Aeronautical Sciences*, vol. 25, Feb. 1958, pp. 73-85.

[25]Landsbaum, E. M., "Thrust of a Conical Nozzle, *ARS Journal*, Vol. 29, March 1959, pp. 212-213.

[26]Driscoll, R. J. and Moon, L. F., "Pressure Recovery in Chemical Lasers," submitted to AIAA J.